The dependence of the tunneling characteristic on the electronic energy bands and the carrier's states of Graphene superlattice

2016 Mater. Res. Express 3 095005

(http://iopscience.iop.org/2053-1591/3/9/095005)

Materials Research Express

RECEIVED
11 May 2016

REVISED
10 August 2016

ACCEPTED FOR PUBLICATION
17 August 2016

PUBLISHED
2 September 2016

PAPER

The dependence of the tunneling characteristic on the electronic energy bands and the carrier's states of Graphene superlattice

C H Yang[1], G Z Shen[1], Z M Ao[2] and Y W Xu[3]

[1] School of Physics and Optoelectronic Engineering, Nanjing University of Information Science and Technology, Nanjing 210044, People's of Republic China
[2] Institute of Environmental Health and Pollution Control, School of Environmental Science and Engineering, Guangdong University of Technology, Guangzhou 510006, People's of Republic China
[3] Science and Technology on Near-Surface Detection Laboratory, Wuxi 214035, People's of Republic China

E-mail: chyang@nuist.edu.cn **and** yewen_xu@126.com

Keywords: graphene superlattice, transfer matrix approach, energy band structure, transport property

Abstract

Using the transfer matrix method, the carrier tunneling properties in graphene superlattice generated by the Thue–Morse sequence and Kolakoski sequence are investigated. The positions and strength of the transmission can be modulated by the barrier structures, the incident energy and angle, the height and width of the potential. These carriers tunneling characteristic can be understood from the energy band structures in the corresponding superlattice systems and the carrier's states in well/barriers. The transmission peaks above the critical incident angle rely on the carrier's resonance in the well regions. The structural diversity can modulate the electronic and transport properties, thus expanding its applications.

1. Introduction

Graphene, a two-dimensional (2D) system with a one-atom-thick sheet of carbon, was fabricated experimentally in 2004 by Geim *et al* [1]. Due to the massless Dirac fermions in graphene, this ultra-thin material exhibits very unique and excellent physical properties, such as, high mobilitie [2], unique quantum Hall effect [1], Klein tunning [3, 4], and so on, which aroused wide investigation on the fundamental physical properties in condensed matter physics in graphene [5–10].

It is well known that the electronic structures can be successfully controlled in superlattices. The interesting system to be considered is the application of a periodic potential to graphene. In graphene-based materials, the superlattice potential structures can be obtained by electrostatic and/or magnetic potential barriers [11–15]. Also, a helium ion microscope was employed to pattern nanoscale grating in fabricating a graphene device [16, 17]. The crystallographic orientation of the nanoribbons was investigated by polarization Raman measurements to give evidence for high-quality patterning process [16]. A series of alternate barriers and wells or graphene superlattice (GSL) $(AB\cdot\cdots\cdots)^N$ with one-dimensional periodic potentials of square barriers are designed. Barriers and wells are labeled as A and B respectively. The electronic band structures and transport properties in GSLs have been extensively investigated [13, 18–25]. Park *et al* investigated the carrier behavior with a periodic potential applied in nanoscale [18]. They found that the dependence of group velocity for states on the wavevector is highly anisotropic which originates from the chiral nature in graphene. Also in the presence of the external periodic potential, gap opening was observed and anisotropic. Wang *et al* investigated the electronic transport properties and energy band structure in $(AB)^N$-GSL [19]. They found a new Dirac point (DP), which corresponds to the zero-averaged wave number $(\bar{k})$, is formed and is only dependent on the ratio of widths of the well and barrier. This opened gap is similar to that in the one-dimensional photonic crystals. The ballistic conductance and the Fano factor are investigated in this $(AB)^N$ structure and the peaks occur in the vicinity of this new DP which originates from transmission probability distribution [20]. Including the energy gap due to the sublattice symmetry breaking, the zero-$\bar{k}$ gap is formed and the related transmission, conductance and Fano factor near this gap are further illustrated [13]. Fibonacci [26, 27] and Thur-Morse [28]

quasi-periodic graphene superlattice structures were designed and the corresponding electronic band gap is investigated which results in the robust transmission properties, conductance and shot noise at the new DPs. The emergence of the extra dirac points located at $k_y \neq 0$ is associated with the variation of the zero-$\bar{k}$ gap. From the above works, they mostly focus on designing the barrier structures and discussing the new DPs and the zero-$\bar{k}$ gap, which can do a comparison with the photonic band gap in photonic crystals. Barbier *et al* analyzed the possible emergency conditions and the positions of these extra DPs in k space [21, 22]. In addition, with magnetic vector potential barriers, the electron transport of asymmetric transmission has been analyzed [14, 15]. In [17], they measured the longitudinal magnetoconductivity at different temperature and gate voltages. A metal to insulator transition was observed. When a sheet of graphene grown on a periodic heterostructure substrate, due to the influence of the substrate, the dependence of both the band gap and the Fermi velocity on the position has been included to the investigation of the electronic energy band structure [27, 29, 30].

During the carrier's transmission process, the carriers moving along the barrier direction are reflected at the well-barrier interface. And the wavevector along the other free direction satisfies the condition of the wavevector conservation, which gives rise to a critical incident angle. Increasing the incident angle and exceeding the critical value, the wavevector becomes imaginary. The carrier states is from the propagating mode to the bound mode which can be used as the waveguide. Therefore, in these quantum well or quantum barrier structures, by an analogy of the optical waveguide, the guided modes for electron waves in graphene are investigated and found that the fundamental mode is absent when both the Klein tunneling and classical motion are present [31, 32]. Similar to graphene superlattice, instead of different barrier layers with alternate dielectric layers containing graphene sheets inserted as a conduction interface, the optical transmission property and field distribution are studied using the transfer matrix method [33–35].

Motivated by these studies, in this paper, we investigate the transmission properties in the graphene-based Thue-Morse and Kolakoski sequences. These barrier structures are more 'disordered' than $(AB)^N$ type. The electronic energy band structure and the carrier states are used to analyze the transport properties. Especially, the transmission peaks above the critical incident angle are investigated. The dependence on the symmetrical and asymmetrical potential structures and the parameters of the potential function has been discussed.

2. Theoretical approaches

The graphene-based periodic-barrier structures are designed as Thue–Morse (TMS) and Kolakoski sequences (KS) along the x direction. The potential profile is one-dimensional configuration with rectangular wells and barriers. The generation of TMS can be seen in [28]. The KS is its own run-length encoding with 1221, 1212, 2122, 1121, ……. Here index 1 (2) indicates well (barrier) layer, respectively. The well and barrier regions are labeled as A and B. The sequence for the former four layers for TMS and KS is same (ABBA) and the following layers are distinctive. The electron dynamics in graphene obeys the 2D massless Dirac equation $H = \gamma\hat{\sigma} \cdot \mathbf{k}$ which differs strongly from the case in a conventional two dimensional electron gas (2DEG) with the kinetic energy proportional to k^2. σ, $\mathbf{k}$ are the pauli matrix operator and wavevector, respectively. The carrier states in a free 2D plane can be expressed by a two-component pseudospinor $\psi(x, y) = \frac{1}{\sqrt{2}}\begin{pmatrix} 1 \\ se^{i\varphi} \end{pmatrix} e^{i(k_x x + k_y y)}$ with φ being the angle between the wavevector $\vec{k} = (k_x, k_y)$ and the x direction. $s = \pm 1$ indicates the conduction band $(+1)$ and valence band (-1). In the applied barrier structure along the x direction, the carries are reflected at the interface. The two side wavefunctions at the interface along the propagation direction refer to the continuity condition and the wave function in well or barrier regions can be written as

$$\psi(x) = a\begin{pmatrix} 1 \\ se^{i\varphi} \end{pmatrix} e^{ik_x x} + b\begin{pmatrix} 1 \\ se^{-i\varphi} \end{pmatrix} e^{-ik_x x} \tag{1}$$

a and b indicate the amplitudes of the forward and backward wavefunction. The carriers can move freely along the y direction which satisfies the conservation of the transversal momentum. Therefore, the transversal momentum $\hbar k_y$ in different region is identical. In order to derive the connection for the wave functions at the interfaces, equation (1) can be written in a matrix as $\psi_i(x) = M_i(x)\begin{pmatrix} a_i \\ b_i \end{pmatrix}$ with $M_i(x) = \begin{pmatrix} e^{ik_{xi}x} & e^{-ik_{xi}x} \\ s_i e^{i\varphi_i} e^{ik_{xi}x} & s_i e^{-i\varphi_i} e^{-ik_{xi}x} \end{pmatrix}$. The index i indicates the different layers, well or barrier. In the well region $k = \frac{E}{\hbar v_F} = \sqrt{k_x^2 + k_y^2}$, $s = sign(E)$. In the barrier region $q = \frac{|E - V|}{\hbar v_F} = \sqrt{q_x^2 + k_y^2}$, $s = sign(E - V)$. V is the height of the barrier. If $k_y > k$ $(k_y > q)$, $k_x = i\sqrt{k_y^2 - k^2}$ $(q_x = i\sqrt{k_y^2 - q^2})$ becomes imaginary. Using this matrix, inside the same layer, the wave function at x and $(x + \Delta x)$ satisfies $\psi(x + \Delta x) = M_i(x + \Delta x) M_i^{-1}(x)\psi(x)$. Using the transfer matrix $M_i(x_R)M_i^{-1}(x_L)$ in a same layer with x_L and x_R being the borders of left and right sides, the transfer matrix in a periodic structure expanded from $(AB \cdot \cdots\cdots)^N$ can be obtained,

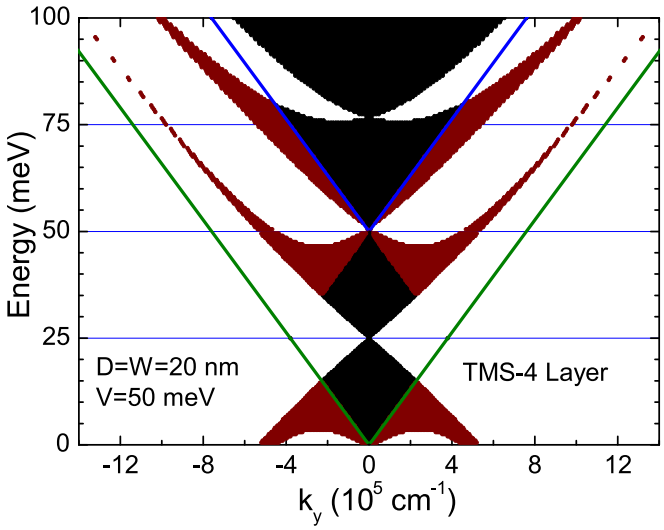

Figure 1. Energy band structure for $(ABBA)^N$ with $D = W = 20$ nm and $V = 50$ meV. The solid green and blue lines indicate the boundary of the linear dispersion relationship in well and barrier, respectively. The black and wine regions correspond to the propagating states and the bound states.

$$X = \Pi_{j=1}^{N} M_i(x_{R_i}) M_i^{-1}(x_{L_i}) \tag{2}$$

$n_A + n_B = N$, n_A and n_B are the layer numbers for well and barrier, respectively. In a $(AB)^N$ periodic structure, the transfer matrix can be simplified as $X = M_B(D + W)M_B^{-1}(D)M_A(D)M_A^{-1}(0)$. The widths of the well and barrier regions are D and W. According to the Bloch's theorem, the electronic dispersion at any incident angle follows the relation

$$2\cos(\beta_x L) = \mathrm{Tr}(X) \tag{3}$$

β_x is the Bloch wavevector. L is the total distance of one periodic unit. In a $(AB\cdot\cdots\cdots)^N$ structure with the first layer being the well region, the reflection (r) and transmission (t) coefficients of the carrier's wave function can be obtained as

$$\begin{pmatrix} 1 \\ r \end{pmatrix} = M_A^{-1}(0) X^{-1} M_A(L) \begin{pmatrix} t \\ 0 \end{pmatrix} \tag{4}$$

Here, the coefficient of the left semi-infinite region $a_1 = 1$, $b_1 = r$. And the coefficient of the right-infinite region $a_{N+1} = t$, $b_{N+1} = 0$. The transmission probability is $T = |t|^2$.

In this paper, the tunneling probability, together with the energy band structure and the carrier's states are investigated in several designed graphene barrier and superlattice structures. The tunneling properties are dependent on the incident energy, incident angle, and the detailed barrier structures. The position and strength of the tunneling can be understood from the energy band structure in the corresponding superlattice systems and the carrier's probability density inside the graphene-based barrier structures.

3. Results and discussions

In this section, the evolution of the transmission, energy band structure, and carrier's probability densities of propagating states and bound states for different generations are investigated. The TMS is ($ABBA$, $BAAB$, $BAAB\cdot\cdot$) and the KS is ($ABBA$, $ABAB$, $ABAA\cdot\cdot$). The structure of the former four layers for TMS and KS is equal followed by different layer structure. It can make an analogy between the results in these two sequences and those in $(AB)^N$ structure.

Figure 1 plots the energy band structure for the potential structure generating by four layers $(ABBA)^N$ of TMS. Here the TMS and KS is equivalent. Actually, it equals to the $(AB)^N$ sequence with double widths. The energy spectrum splits into several subbands and is symmetric with respect to the transverse wavevector $k_y = 0$. The new Dirac point locates at $\bar{k} = \Sigma_{i=1}^{N} k_i w_j / \Sigma_{i=1}^{N} w_j = 0$ [28]. Since the number of well and barrier is same, it is easy to obtain the energy for $\bar{k} = 0$ as $E = V/(1 + D/W)$ which depends only on the ratio of D/W instead of the barrier and well widths. In figure 1, $D = W = 20$ nm and $V = 50$ meV, the energy for the new Dirac point is $E_{DP} = 25$ meV which is consistent with the [19]. The energy subband curves above/below the new Dirac point bends upward/downward. When $E < V$, it denotes the interband scattering at the well/barrier interface with electron states in well and hole states in barrier. The energy band structures between $(0,\ V/2)$ and

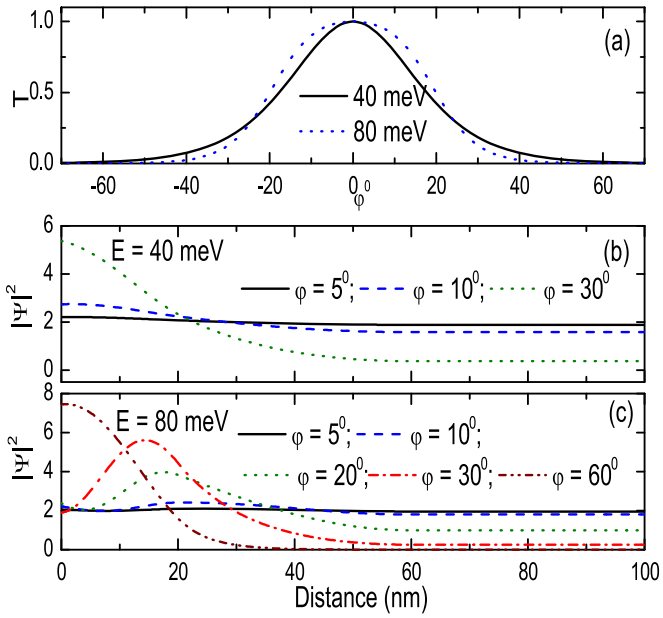

Figure 2. (a) Transmission probability as a function of the incident angle at finite incident energy $E = 40$ meV and $E = 80$ meV. The evolution of the probability density $|\psi|^2$ inside the graphene-based barrier structures with different incident angles (b) (c). The other parameters are the same as those in figure 1.

$(V/2,\ V)$ is symmetric with respect to $E = V/2$. The states at $(E,\ V - E)$ or $(V - E,\ E)$ for $E < V$ are the matching electron and hole states with the equal wavevector k. When $E > V$, the carriers are influenced by the barrier structure and the intraband scattering occurs with both electron states in well and barrier. In this figure, the solid green and blue lines indicate the boundary of the linear dispersion relationship in well and barrier, respectively. Therefore, the wavevector k_x is real within these boundaries colored in black in figure 1 denoting the propagating states, and the wavevector k_x or q_x is imaginary beyond these boundaries colored in wine denoting the bound states in well and barrier regions. The bound states in quantum well play the roles of guide modes along the channel [36]. When the carriers traversing a barrier structure, the incident wavevector k_x is real. There is a critical angle $\varphi_c = \texttt{arcsin}(|E - V|/E)$. When the incident angle is less than φ_c, the carriers moving through the barrier are propagating states. While increasing the incident angle larger than φ_c, the wavevector q_x in barrier becomes imaginary, and the carriers are bounded. The corresponding transmission probability as a function of the incident angle at a given incident energy is shown in figure 2(a). When the incident electron energy is 40 meV or 80 meV, the transmission probability shows an obvious tunneling region at about $(-40^\circ,\ 40^\circ)$. At the normal incident case, the transmission probability tends to 1 which is a reflection of Klein tunneling. The critical angle $\varphi_c = 14.48^\circ,\ 22.02^\circ$ at $E = 40$ meV and 80 meV, respectively. When the incident angle exceeds this critical angle, the carriers still can be transmitted and the transmission probability decreases with increasing the angle continuously. In the energy band spectrum of figure 1, three parts for carrier states at $E = 80$ meV can be obtained, i.e., about $(-10^\circ,\ 10^\circ)$ the propagating states, at about $\pm 30^\circ$ and $\pm 60^\circ$ the bound states. The wave function probability density in figures 2(b) and (c) reflects an obvious reflection when the incident angle above the critical angle. Decreasing the incident angle to the normal incidence, the electrons can move through the barriers with less reflection.

Increasing the number of layers in periodic unit, the energy band in figure 3 is depicted. Comparing the spectrum in figure 1, the number of the energy subbands is increasing, which appears the rich energy band spectrum. The former 8 layers for TMS are (*ABBA*, *BAAB*) and for KS are (*ABBA*, *ABAB*). There is only different between the 5th and 6th layers *AB* or *BA*. However, the distinct energy bands can be seen that there are more subbands in KS than those in TMS which offers the carriers more opportunities to transmit through the barrier structures. The main difference for the energy band structure is at the incident energy $E = V$. When $E = V$, the real solution for β_x occurs only at normal incident case ($\varphi = 0$). Near the normal incidence, the wavevector becomes imaginary in the barrier region and the bound states are only observed in the case of TMS. This state solutions at $E = V$ are similar to the figure 2 in [19]. Therefore, the energy band depends on the detailed well/barrier structure in each periodic unit. The corresponding transmission probability and the evolution of the probability density $|\psi|^2$ inside the graphene-based barrier structures are shown in figures 4 and 5. The numerical results for TMS and for KS can be compared. The transmission probability is symmetrical with respect to the normal incidence. The transmission curves for KS exhibit rich transmission patterns. When the incident angle

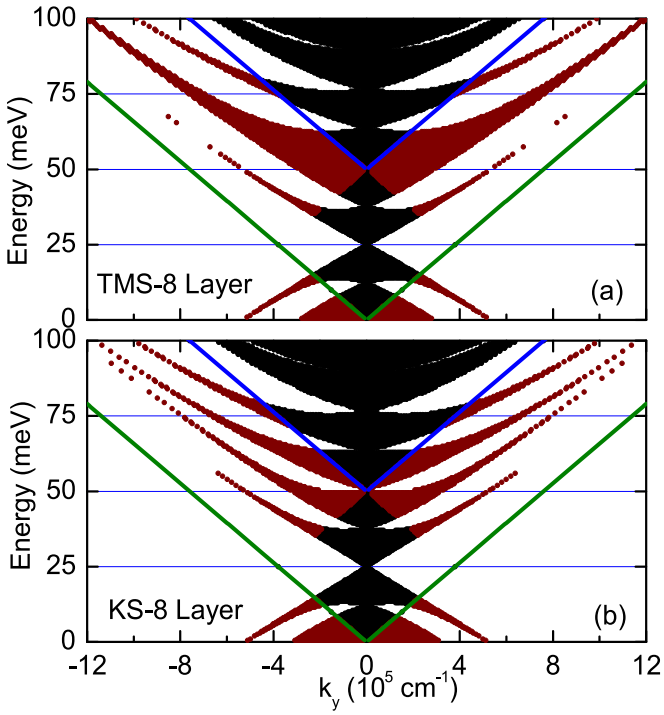

Figure 3. Energy band structures in the periodic well/barrier generated by 8 layers of TMS $(ABBA,\ BAAB)^N$ and KS $(ABBA,\ ABAB)^N$. The information for the solid green, blue lines the black and wine regions in figures and the other parameters are the same as those in figure 1.

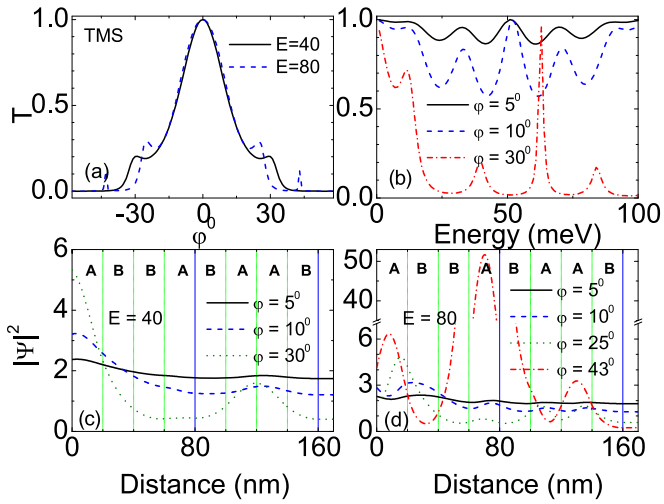

Figure 4. Transmission probability for TMS as a function of the incident angle at a finite incident energy E (a) and as a function of the incident energy at a given incident angle (b). The evolution of the probability density $|\psi|^2$ inside the graphene-based barrier structures with different incident angles at a given incident energy $E = 40$ meV (c) and $E = 80$ meV (d). The other parameters are the same as those in figure 3.

from 0 to about $\pm\varphi_c$, the transmission probability decreases from '1' continuously. Above the critical angle $|\varphi_c|$, there are several transmission peaks can be observed. These transmission probability could even approach unity in KS structure in figure 5(a). These transmission peaks can also be seen for the incident energy dependence of the transmission probability in figures 4(b) and 5(b) when incident angle $\varphi = 30^\circ > \varphi_c$. When the incident angle is relatively small, the transmission probability oscillates with a finite value. Because of $\bar{k}-$ energy gap, the dip transmitivity at the new DP ($E_{DP} = 25$ meV) can be observed. When the incident energy $E = V$, the transmission probability is close to 1 at small angle incidence and decreases with increasing the incident angle. The transmission curves can be understood from the probability density for wave function in well/barrier structures. When the incident angle below the critical angle, the reflection amplitude is small and the carriers

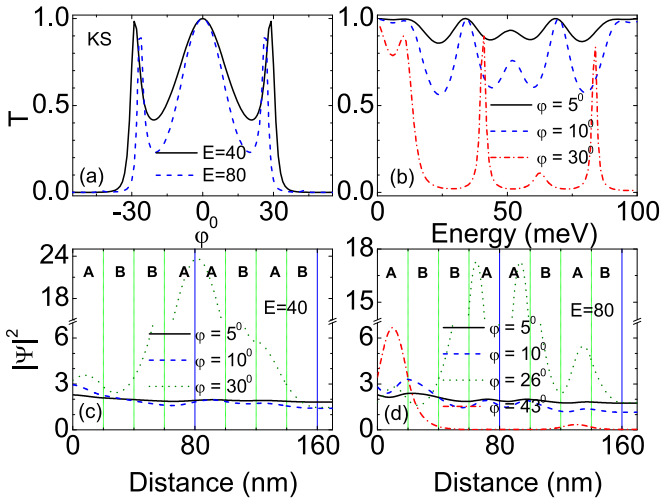

Figure 5. The same as the figure 4 but for the case of KS.

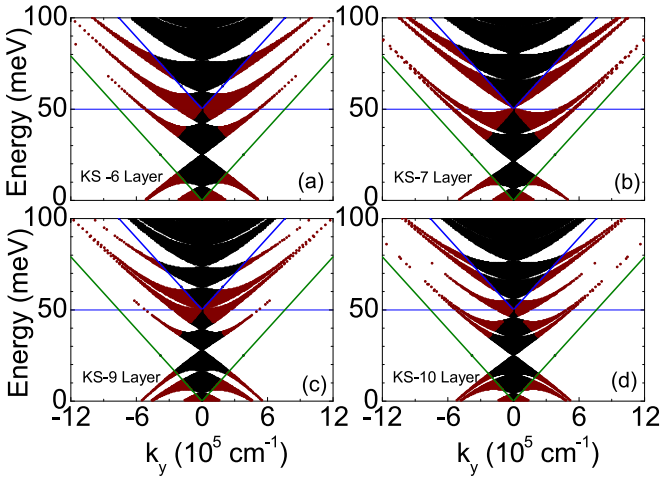

Figure 6. Energy band structures in the periodic well/barrier generated by 6, 7, 9, or 10 layers for KS $(ABBA,\ ABAB,\ BA)^N$. The information for the solid green, blue lines, the black and wine regions in figures and the other parameters are the same as those in figure 1.

close to normal incidence could pass through the barriers. While above the $|\varphi_c|$, the carrier's probability density is highly localized inside the middle well regions or the carrier states have a strong reflection which arises the phenomena of transmission peaks. I.e., $\varphi = 30°$ when $E = 40$ meV in figures 4(c) and 5(c), $\varphi = 25°,\ 43°$ when $E = 80$ meV in figure 4(d), and $\varphi = 26°,\ 43°$ when $E = 80$ meV in figure 5(d).

In figure 6, it shows the energy band structure of KS for different well layers. Comparing figures 6(a) and (b), (c) and (d), the 7th and 10th layers are well region. This extra well layer induces the distinct energy band for the corresponding periodic well/barrier structures. And the new DPs for zero- $\bar{k}$ is different which is depends on the layer numbers of well and barrier. The DP locates at 25 meV for the same layer number of well and barrier in figures 6(a) and (d). While the DPs locate at 21.43 meV for 4 layer well and 3 layer barrier in figure 6(b) and 27.78 meV for 4 layer well and 5 layer barrier in figure 6(c), respectively. Increasing the barrier layer number, the location for the new DP increases. Although there is a difference in the periodic structure units in figures 6(a) and (b), (c) and (d), the electrons encounter the same barrier structures when carriers transmit from one side to the other side, which has the same transport behavior in figure 7. The extra well layers have no influence on the carrier transmission property. The related transmission probability at a given incident energy has been shown as a function of the incident angle. From the normal incidence to the oblique incidence, the declining transmission can be observed with several peaks at some extra angles above the critical angle. The related carrier probability densities $|\psi|^2$ during the tunneling process have been shown in figures 7(b) and (d). The strong localized states in well regions represents the carrier resonance phenomenon, which arises the transmission peaks.

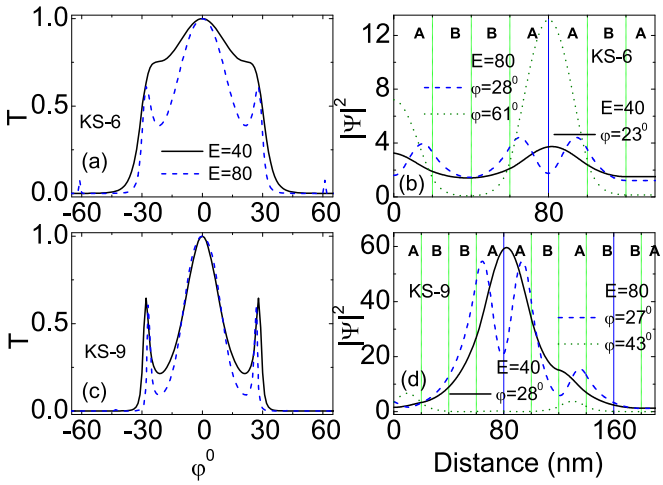

Figure 7. Transmission probability for KS as a function of the incident angle at a finite incident energy E for different transmission barrier units (a)(c). The corresponding evolution of the probability density $|\psi|^2$ inside the graphene-based barrier structures with different incident angles at a given incident energy $E = 40$ meV and $E = 80$ meV in (b)(d). The well/barrier structure units are from figure 6.

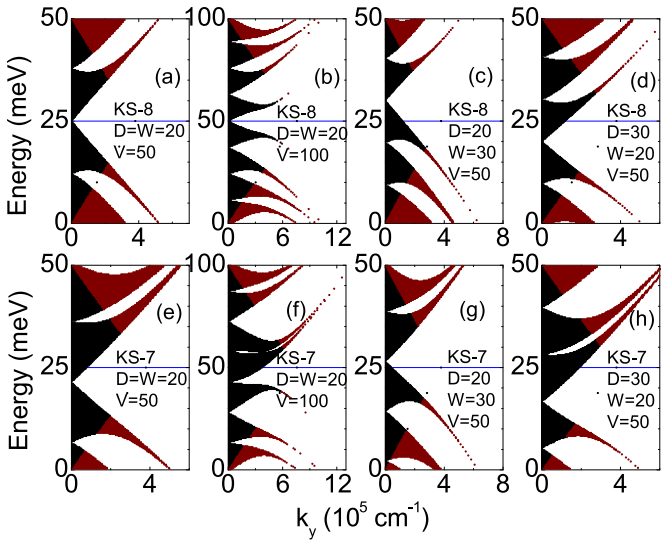

Figure 8. Energy band structures generated by 8 (a)–(d) and 7 (e)–(h) layers of KS for (a) (e) D = W = 20 nm, V = 50 meV, (b) (f) D = W = 20 nm, V = 100 meV, (c) (g) D = 20 nm, W = 30 nm, V = 50 meV, and (d) (h) D = 30 nm, W = 20 nm, V = 50 meV. The black and wine regions correspond to the propagating states and the bound states.

In figure 8, modulating the height and the width of the well and barrier, we plot the energy band structures for two kinds of potential structures generated by 8 and 7 layers of KS. In each periodic unit, the layer number for well and barrier is same $n_A = n_B = 4$ for the generating case of 8 layers, and is different $n_A = 4$, $n_B = 3$ for the generating case of 7 layers. The rich and modulated energy band spectrums give rise to various carrier transmission properties which depend on these parameters.

In summary, using the transfer matrix approach we have theoretically studied the energy band spectrum, transmission and the carrier states in TMS and KS barrier structures. The new Dirac point which corresponds to the zero averaged wave number depends on the width ratio and the layer number of the well/barrier. Away from the normal incidence, the zero-$\bar{k}$ energy gap can be observed. During the carrier transmitting process along the barrier structures, the wavevector along the other free direction of the 2D plane satisfies the condition of the conservation and the critical incident angle distinguishes the propagating states and the bound states. The transmission probability T is symmetrical with respect to the normal incidence. $T = 1$ at the normal incidence represents the Klein tunneling. Increasing the incident angle, the transmission probability decreases with several possible emergent peaks above the critical angle. These appeared peaks for the detailed structure parameters can be understood from the carrier's probability density inside the potential structures. These peaks originate from

the probability density localized inside the well regions with the occurrence of the resonance. The carrier transmission property can be analyzed from the energy band spectrum with the periodic potential structure generated by the carrier transmitting well/barrier unit and the carrier's probability density. There has no influence on the tunneling property with extra well layers at one side of the periodic unit. Therefore, more periodic potential units can be designed to obtained the energy band structures to analyze the tunneling windows, approximately. Increasing the width and/or decreasing the height of the potential barrier, the more subbands in the energy band will tend to quasi continuous band and the transport properties will exhibit much homogeneous. In our numerical calculation, the height and the width of the potential barrier, the equal or unequal layer number of well/barrier, and the detailed barrier sequences can be used to modulate the energy band spectrums and transport properties.

Acknowledgments

This work was supported by the Natural Science Foundation of Jiangsu Province (BK20131428), the Scientific Research Foundation for the Returned Overseas Chinese Scholars from State Education Ministry of China and the Qing-Lan Project of Jiangsu Province (Yang). The National Science Foundation of China (11547030). Z Ao acknowledges the financial supports from '100 talents' program of Guangdong University of Technology, and '1000 plan' for young professionals program of Chinese Government.

References

[1] Novoselov K S, Geim A K, Morozov S V, Jiang D, Katsnelson M I, Grigorieva I V, Dubonos S V and Firsov A A 2005 *Nature (London)* **438** 197–200
Zhang Y, Tan Y-W, Stormer H L and Kim P 2005 *Nature (London)* **438** 201–4
[2] Morozov S V, Novoselov K S, Katsnelson M I, Schedin F, Elias D C, Jaszczak J A and Geim A K 2008 *Phys. Rev. Lett.* **100** 016602
[3] Katsnelson M I, Novoselov K S and Geim A K 2006 *Nat. Phys.* **2** 620
[4] Sonin E B 2009 *Phys. Rev.* B **79** 195438
[5] Neto A H C, Guinea F, Peres N M R, Novoselov K S and Geim A K 2009 *Rev. Mod. Phys.* **81** 109–62
[6] Das S, Adam S, Hwang E H and Rossi E 2011 *Rev. Mod. Phys.* **83** 407–70
[7] Kotov V N, Uchoa B and Pereira V M 2012 *Rev. Mod. Phys.* **84** 1067–125
[8] Roldán R, Goerbig M O and Fuchs J-N 2010 *Semicond. Sci. Technol.* **25** 034005
[9] e.g., Morimoto T, Hatsugai Y and Aoki H 2008 *Phys. Rev.* B **78** 073406
Hwang E H and Sarma S Das 2009 *Phys. Rev.* B **79** 165404
Wright A R and Zhang C 2010 *Phys. Rev.* B **81** 165413
[10] e.g., Faugeras C, Amado M, Kossacki P, Orlita M, Sprinkle M, Berger C, de Heer W A and Potemski M 2009 *Phys. Rev. Lett.* **103** 186803
Orlita M and Potemski M 2010 *Semicond. Sci. Technol.* **25** 063001
[11] Huard B, Sulpizio J A, Stander N, Todd K, Yang B and Gordon D G 2007 *Phys.Rev.Lett.* **98** 236803
[12] Stander N, Huard B and Gordon D G 2009 *Phys.Rev.Lett.* **102** 026807
[13] Wang L G and Chen X 2011 *J. Appl. Phys.* **109** 033710
[14] Ghosh S, Sharma M and Phys J 2011 *Condens. Matter* **23** 55501
[15] Ghosh S, Sharma M and Phys J 2009 *Condens. Matter* **21** 292204
[16] Archanjo B S, Fragneaud B, Canc??ado L G, Winston D, Miao F, Achete C A and Medeiros-Ribeiro G 2014 *Appl, Phys. Lett.* **104** 193114
[17] Araujo E N D, Brant J C, Archanjo B S, Medeiros-Ribeiro G, Plentz F and Alves E S 2015 *Phys. Rev.* B **91** 245414
[18] Park C, Yang L, Son Y, Cohen M L and Louie S G 2008 *Nat. Phys.* **4** 213
[19] Wang L-G and Zhu S-Y 2010 *Phys. Rev.* B **81** 205444
[20] Guo X X, Liu D and Li Y X 2011 *Appl. Phys. Lett* **98** 242101
[21] Barbier M, Vasilopoulos P and Peeters F M 2010 *Phys. Rev.* B **81** 075438
[22] Barbier M, Vasilopoulos P and Peeters F M 2010 *Phil. Trans. R. Soc.* A **368** 5499
[23] Bai C X and Zhang X D 2007 *Phys. Rev.* B **76** 075430
[24] Barbier M, peeters F M, Vasilopoulos P and Pereira J M Jr 2008 *Phys. Rev.* B **77** 115446
[25] Xu Y, He Y and Yang Y F 2015 *Physica* B **457** 188
[26] Zhao P L and Chen X 2011 *Appl. Phys. Lett* **99** 182108
[27] García-Cervantes H, Madrigal-Melchor J, Martínez-Orozco J C and Rodríguez-Vargas I 2015 *Physica* B **478** 99
[28] Ma T X, Liang C, Wang L G and Lin H Q 2012 *Appl. Phys. Lett.* **100** 252402
[29] Lina J R F and Moraes F 2015 *Solid State Commun.* **201** 82
[30] Briones-Torres J A, Madrigal-Melchor J, Martínez-Orozco J C and Rodríguez-Vargas I 2014 *Superlattices Microstruct.* **73** 98–112
[31] He Y *et al* 2015 *Superlattices Microstruct.* **85** 761
[32] He Y *et al* 2014 *Appl. Phys.* A **115** 895–902
[33] Zhang L *et al* 2016 *Optik* **127** 2030–5
[34] Entezar S R, Saleki Z and Madani A 2015 *Physica* B **478** 122–6
[35] Zhang Y *et al* 2015 *Opt. Commun.* **338** 168–73
[36] Wu Z 2011 *Appl. Phys. Lett.* **98** 082117